# Theoretical Study on the Reaction Mechanism of NH 2 − with O 2 (a 1 Δ g )

**ARTICLE** *in* THE JOURNAL OF PHYSICAL CHEMISTRY A · NOVEMBER 2011

Impact Factor: 2.69 · DOI: 10.1021/jp206518j · Source: PubMed



**7 AUTHORS**, INCLUDING:

Dan Li
Shantou University
**156** PUBLICATIONS **4,323** CITATIONS
SEE PROFILE

Xiao-Chun Huang
Shantou University
**72** PUBLICATIONS **3,671** CITATIONS
SEE PROFILE

THE JOURNAL OF PHYSICAL CHEMISTRY A

ARTICLE

pubs.acs.org/JPCA

# Theoretical Study on the Reaction Mechanism of $NH_2^-$ with $O_2$ ($a^1\Delta_g$)

Hai-xia Lin,[†] Guang-hui Chen,*[,†] Hui-ling Liu,[‡] Dan Li,[†] Xiao-chun Huang,[†] Wen-guang Liu,[†] and Yu-qiu Jiao[§]

[†]Department of Chemistry, Shantou University, Guangdong 515063, People's Republic of China

[‡]State Key Laboratory of Theoretical and Computational Chemistry, Institute of Theoretical Chemistry Jilin University, Changchun 130023, People's Republic of China

[§]College of Science, China University of Petroleum, Changping, Beijing 102249, People's Republic of China

**ABSTRACT:** A detailed theoretical study of the potential energy surface of poorly understood ion−molecule reaction of $NH_2^-$ and $O_2$ ($a^1\Delta_g$) is explored at the density functional theory B3LYP/6-311++G(d,p), ab initio of QCISD/6-311++G(d,p) and CCSD(T)/6-311++G(3df, 2pd) (single-point) theoretical levels for the first time. It is shown that there are six total possible products from $\mathbf{P_1}$ to $\mathbf{P_6}$ on the singlet potential energy surface. Among these, the charge-transfer product $\mathbf{P_1}$ ($NH_2 + O_2^-$) is the most favorable product with predominant abundances, whereas $\mathbf{P_4}$ ($NO^- + H_2O$) and $\mathbf{P_2}$ ($HNO + OH^-$) may be the second and third feasible products followed by the almost neglectable $\mathbf{P_3}$ ($NO_2^- + H_2$), while $\mathbf{P_5}$ (c-$NO_2^- + H_2$) and $\mathbf{P_6}$ ($ONO^- + H_2$) will not be observed due to their either high barriers or being secondary products. The present theoretical study points out that besides $\mathbf{P_1}$ ($NH_2 + O_2^-$) and $\mathbf{P_2}$ ($HNO + OH^-$), $\mathbf{P_4}$ ($NO^- + H_2O$) should be also observed, which is different from the previous experiment study by Anthony Midey et al. in 2008. In addition, almost all of the reaction pathways to products are exothermic and the reaction rate should be very fast since the reaction barriers are very low except for $\mathbf{P_5}$ (*c*-$NO_2^- + H_2$) which is in agreement with the measured total reaction rate constant $k = 9.0 \times 10^{-10}$ $cm^3s^{-1}$ at 300 K in the experiment study. It is expected that the present theoretical study may be helpful for the understanding of the reaction mechanism related to $NHX^-$, $NX_2^-$, $PHX^-$, and $PX_2^-$ (X = H, F, and Cl).

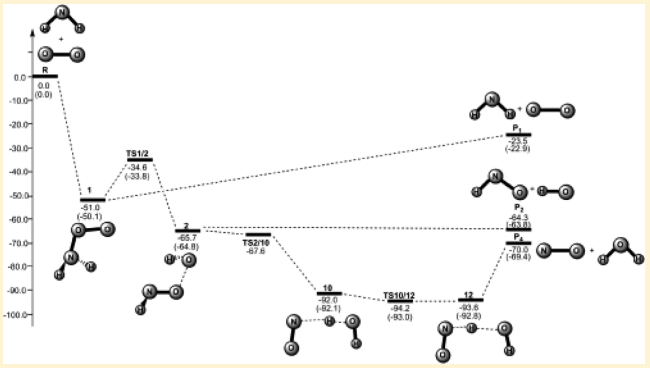


## 1. INTRODUCTION

Ammonia gas is a kind of important gas in the atmosphere,[1] which is the main raw material to synthesize nitrogen fertilizer in agriculture and is also used for making fiber, plastic and dyestuff etc., industrially. In recent years, $NH_2^-$, which can be produced by $NH_3$ under conditions of negative charges or alkali,[2−6] has been a research focus on ion−molecule of gas phase chemical reaction.[7−13] In 1995, Satoshi Okada and Yasuo Abe studied the potential energy surfaces (PESs) of Gibbs free energies of gas phase reactions of $NH_2^-$ + $N_2O$ and $NH_2^-$ + $CO_2$ theoretically.[14] Their major concern is the reversal of exothermicities and reaction rates of these two reactions and their theoretical studies have clarified all of the elementary processes and free energy changes of $NH_2^-$ + $N_2O$ and $NH_2^-$ + $CO_2$ reactions. In addition, Mikael Perakyla studied on the proton abstraction from acetaldehyde by the first and second row hydride anions $NH_2^-$ et al.,[15] using ab initio quantum mechanical calculations.

However, electronically excited molecular oxygen $O_2$ ($a^1\Delta_g$) has an important photochemical and biological implication, which plays a key role in photodynamic therapy for the treatment of cancer.[16] The lowest-lying singlet state of molecular oxygen, $O_2$ ($a^1\Delta_g$), is prevalent in both the quiescent and aurorally excited lower ionosphere, which is formed by a combination of photo dissociation of $O_3$ and direct electron excitation.[17] Although appreciable concentration of $O_2$ ($a^1\Delta_g$) has been observed in the ionosphere, little is known about the reactivity of this species in the gas phase.[18] In 2008, Anthony Midey et al.[19] measured the rate constants and product branching ratios for the reactions of negative ions $NH_2^-$ etc. with $O_2$ ($a^1\Delta_g$) by the selected ion flow tube (SIFT) technology, and it is shown that the extra electron of $NH_2^-$ can transfer rapidly to $O_2$ ($a^1\Delta_g$) to produce the favorable product $\mathbf{P_1}$ ($NH_2 + O_2^-$) followed by few $\mathbf{P_2}$ ($HNO + OH^-$). The measured rate constant at 300 K is $k = 9.0 \times 10^{-10}$ $cm^3s^{-1}$, and products and distribution experimentally are listed as follows:

$$NH_2^- + O_2(a^1\Delta g) \rightarrow NH_2 + O_2^- \geq 0.95$$

$$\rightarrow HNO + OH^- \leq 0.05$$

However, without establishing the PES of $NH_2^-$ + $O_2$ ($a^1\Delta_g$), it is impossible to interpret the reaction mechanism. In this work, the ion−molecule reaction of $NH_2^-$ and $O_2$ ($a^1\Delta_g$) is investigated for the first time by establishing a complete PES using the quantum chemical calculation method.

**Received:** July 10, 2011
**Revised:** October 6, 2011
**Published:** October 07, 2011





dx.doi.org/10.1021/jp206518j | *J. Phys. Chem. A* 2011, 115, 13581–13588

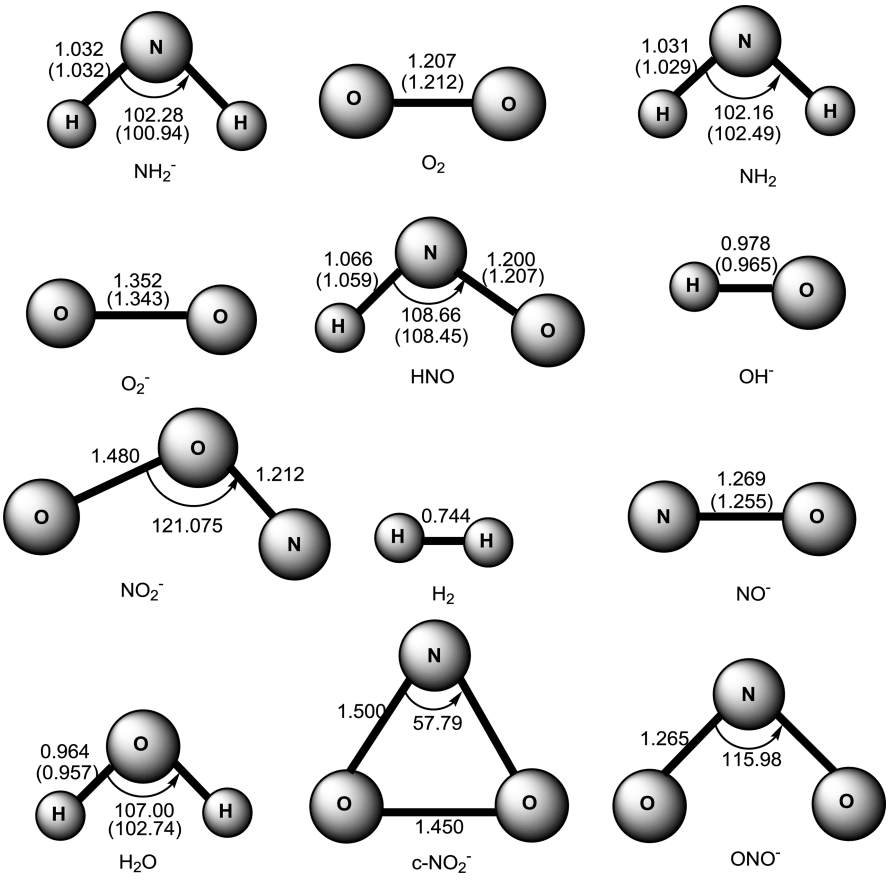


**Figure 1.** The optimized structures of reactants and products of reaction $NH_2^- + O_2$ ($a^1\Delta_g$) in singlet state at the B3LYP/6-311++G(d,p) level. Bond lengths are in angstroms and angles in degrees; the values in parentheses are at the QCISD/6-311++G(d,p) level.

## 2. COMPUTATIONAL METHODS

All of the calculations in this work were performed with the Gaussian03 suite of programs.[20] The species found on the PES were characterized by harmonic frequency calculations at the density functional theory (DFT) level, employing the hybrid Becke three-parameter Lee−Yang−Parr exchange correlation functional (B3LYP)[21,22] with the standard 6-311++G(d, p) basis set.[23−25] If the structures have positive definite Hessian matrices, then the species was identified as stationary points, while transition structures (TSs) show only one negative eigenvalue in their diagonalized force constant matrices. Connectivity of the optimized transition state structures with the corresponding isomers was verified by following the reaction coordinate backward and forward, respectively, using the intrinsic reaction coordinate method (IRC).[26] The zero-point vibrational energy (ZPVE) corrections were computed at the B3LYP/6-311++G(d, p) level. To obtain more reliable energies, the single-point of coupled cluster singles and doubles perturbative estimate of triples [CCSD(T)][27,28] calculations were carried out on the B3LYP/6-311++G(d, p) geometries using the 6-311++G(3df, 2pd)[29] basis set, which is simplified as CCSD(T)//B3LYP. For the species on the favorable pathways, to obtain more reliable geometrical structures and relative energies, further QCISD[30] optimization calculations which includes high-level electron correlation were also employed and correspondingly the single-point calculations were denoted as CCSD(T)//QCISD.

## 3. RESULTS AND DISCUSSION

For the conciseness, the optimized structures of reactants and products at the B3LYP/6-311++G(d,p) and QCISD/6-311++G(d,p) levels are shown in Figure 1, while that of intermediates and transition states obtained at the same levels are depicted in Figure 2, where the eigenvectors of the imaginary frequencies are denoted by arrows; by means of connection of reactants, intermediates, transition states, and products, the schematic PES of the title reaction at the CCSD(T)//B3LYP and CCSD(T)//QCISD levels are plotted in Figure 3; the energetic data for various species involved on the PES at the B3LYP/6-311++G(d, p) and QCISD/6-311++G(d,p) levels are listed in Table 1, where the imaginary frequencies for all the transition states calculated at the B3LYP/6-311++G(d,p) level are listed also. For convenient discussion, the total energy of the reactant **R** ($NH_2^- + O_2$) is set as zero for reference and the symbol **TSm/n** indicates the transition state connecting isomers **m** and **n**.

**3.1. Initial Association.** $NH_2^-$ was optimized at the B3LYP/6-311++G(d,p) level with $C_{2v}$ symmetry with the negative charge mainly concentrated on N ($-1.522e$) atom, which can be viewed as the active site of $NH_2^-$ as shown in Figure 1. On both singlet and triplet PESs, the association of $O_2$ ($a^1\Delta_g$) with $NH_2^-$ may have only one pattern, i.e., the nucleophile $NH_2^-$ should attack the O of $O_2$ ($a^1\Delta_g$) to form singlet complex **1** ($H_2NO_2^-$) and triplet complex $^3$**1** ($H_2NO_2^-$) as shown in Figure 2, which are energetically 51.0 and 5.0 kcal/mol below reactants **R**, respectively, as shown in Figure 3. Note that the

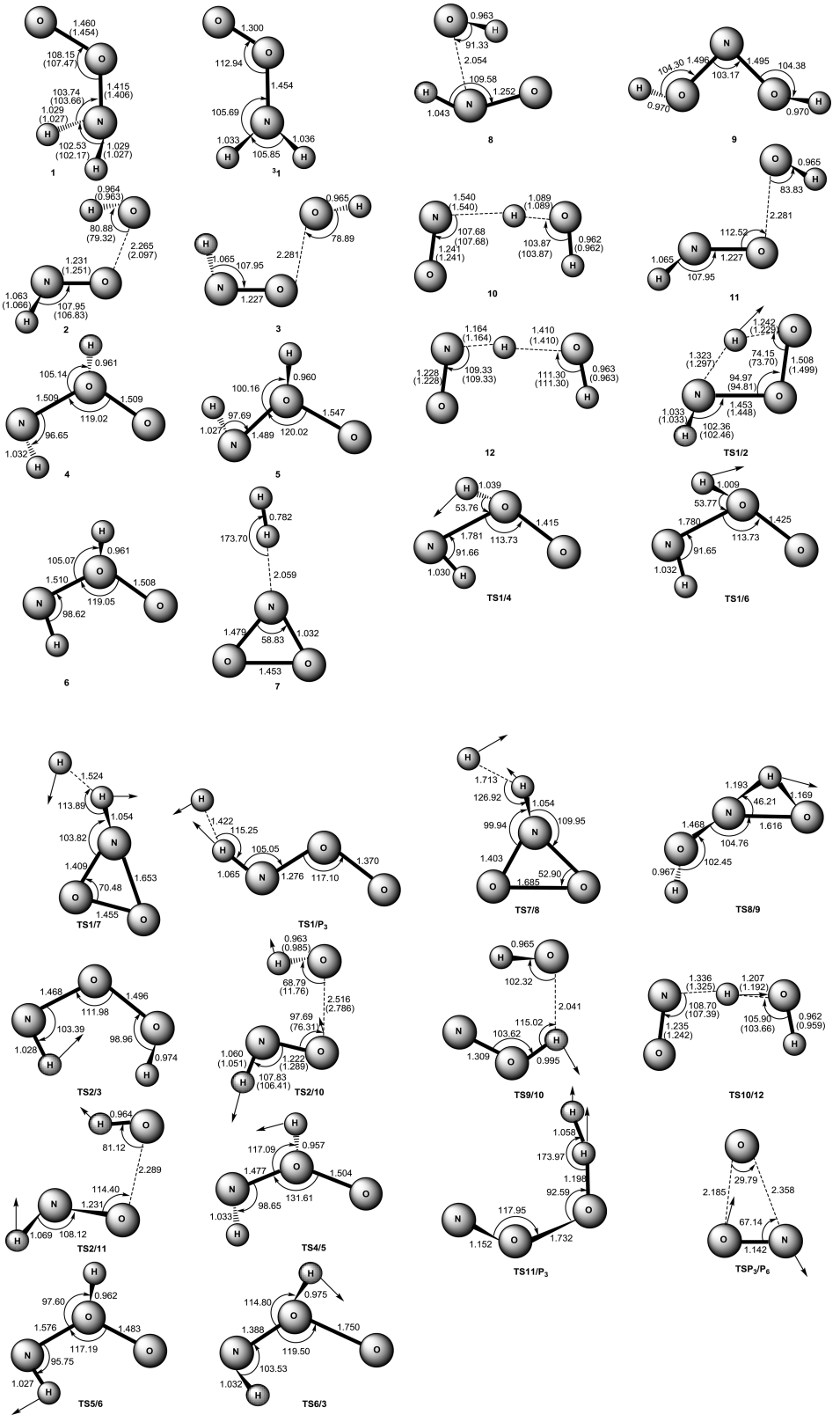


**Figure 2.** The optimized structures of intermediates and transition states of reaction $NH_2^- + O_2$ ($a^1\Delta_g$) in singlet state at the B3LYP/6-311++G(d, p) level. Note that $^3$**1** is a complex in triplet state. Bond lengths are in angstroms and angles in degrees; the values in parentheses are at the QCISD/6-311++G(d, p) level.

lengths of O−N bonds in **1** ($H_2NO_2^-$) and $^3$**1** ($H_2NO_2^-$) are 1.415 and 1.454 Å, respectively. Complex **1** should be thermodynamically more favorable than $^3$**1** due to its much lower relative energy. So, in the following part, we will just discuss the formation pathways of various products associated with complex **1** on the singlet PES. To determine whether there exists any transition

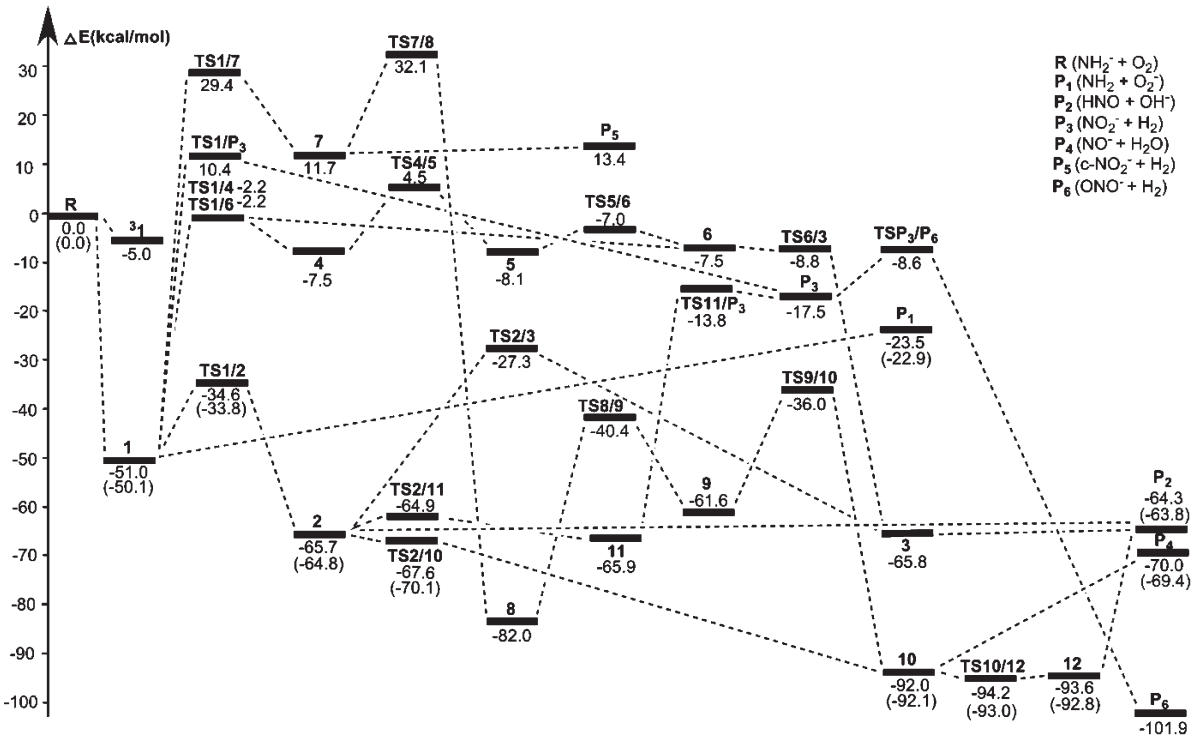


**Figure 3.** The sketch map of the potential energy surface of reaction $NH_2^- + O_2$ ($a^1\Delta_g$) at the CCSD(T)/6-311++G(3df, 2pd)//B3LYP/6-311++G(d, p) level; the values in parentheses are at the QCISD/6-311++G(d, p) level.

state between **R** and **1**, the potential energy curve with variation of the bond length of N−O of **1** is plotted as shown in Figure 4a. It is clear that no transition state can be found during the variation of the N−O bond length, indicating that from reactants **R** to the complex **1** is a barrierless process.

**3.2. Isomerization and Dissociation.** At the B3LYP/6-311++G(d, p) level, totally six dissociation products including $\mathbf{P_1}$ ($NH_2 + O_2^-$), $\mathbf{P_2}$ (HNO + OH−), $\mathbf{P_3}$ ($NO_2^- + H_2$), $\mathbf{P_4}$ ($NO^- + H_2O$), $\mathbf{P_5}$ (c-$NO_2^-$ + $H_2$), and $\mathbf{P_6}$ ($ONO^- + H_2$) from complex **1**($H_2NO_2^-$) can be obtained on the singlet PES as shown in Figure 3. Among these, only $\mathbf{P_5}$ (c-$NO_2^-$ + $H_2$) (13.4 kcal/mol) is energetically higher than the reactants (**R**), whereas remaining $\mathbf{P_1}$, $\mathbf{P_2}$, $\mathbf{P_3}$, $\mathbf{P_4}$, and $\mathbf{P_6}$ are energetically 23.5, 64.3, 17.5, 70.0, and 101.9 kcal/mol below the reactants (**R**), respectively. We now analyze the isomerization and dissociation channels to each product in detail as follows:

$\mathbf{P_1}(NH_2 + O_2^-)$

$\mathbf{P_1}$ ($NH_2 + O_2^-$) may be a charge-transfer product with respect to **R** ($NH_2^- + O_2$), since it is thermodynamically feasible due to the fact that our calculated electron affinity (EA) of 37.9 kcal/mol for $O_2$ ($a^1\Delta_g$) is much larger than that of 17.8 kcal/mol for $NH_2$ at the G2 level.[31] In addition, it is shown that no transition state can be found during elongation of N−O distance as plotted in Figure 4a. Therefore, $\mathbf{P_1}$ ($NH_2 + O_2^-$), which is energetically 23.5 kcal/mol lower than reactants, can be obtained via direct N−O rupture of complex **1** without any barrier. This exothermic process may be generated via long-range collision, and should be a competitive channel.

$\mathbf{P_1}$ : **R** → **1** → $\mathbf{P_1}$

$\mathbf{P_2}(HNO + OH^-)$

From the singlet complex **1** ($H_2NO_2^-$), there are totally six possible pathways to $\mathbf{P_2}$:

$\mathbf{P_2}(1)$ : **R** → **1** → **2** → $\mathbf{P_2}$

$\mathbf{P_2}(2)$ : **R** → **1** → **2** → **3** → $\mathbf{P_2}$

$\mathbf{P_2}(3)$ : **R** → **1** → **2** → **10** → **12** → $\mathbf{P_2}$

$\mathbf{P_2}(4)$ : **R** → **1** → **6** → **3** → $\mathbf{P_2}$

$\mathbf{P_2}(5)$ : **R** → **1** → **4** → **5** → **6** → **3** → $\mathbf{P_2}$

$\mathbf{P_2}(6)$ : **R** → **1** → **7** → **8** → **9** → **10** → **12** → $\mathbf{P_2}$

At first, complex **1** ($H_2NO_2^-$) can pass a 1,3-H-shift barrier (**TS1/2**) at 16.4 kcal/mol to generate intermediate **2** ($HNO\cdots OH^-$), then dissociate directly to $\mathbf{P_2}$ ($HNO + OH^-$) barrierlessly as indicated in $\mathbf{P_2}(1)$, which can be confirmed by the pointwise dissociation potential energy curve as shown in Figure 4b. However, **2** can take the other two pathways to $\mathbf{P_2}$, i.e., by means of rotation and elongation of the O−O bond, **2** will cross a barrier of 38.4 kcal/mol to form an intermediate **3** ($HNO\cdots OH^-$) before $\mathbf{P_2}$ ($HNO + OH^-$) as shown in $\mathbf{P_2}(2)$; at the same time, isomer **2** can also take a barrierless 1,3-H-shift (H transfers from N to O) process to form **10** ($ON\cdots H_2O^-$) followed by a elongation of H−O bond to form **12** ($ON\cdots H\cdots OH^-$) before $\mathbf{P_2}$ ($HNO + OH^-$) as listed in pathway $\mathbf{P_2}(3)$. Note that the **TS2/10** and **TS10/12** are energetically slightly lower than isomers **2**, **10**, and **12** on the PES, respectively, which should result from the higher-level single-point [CCSD(T)/6-311++G(3df, 2pd)] calculations at the lower-level [B3LYP/6-311++G(d, p)] optimized geometries.

**Table 1. Relative Energies (kcal/mol) of the Reactants, Products, Intermediates and Transition States for the $NH_2^- + O_2$ ($a^1\Delta_g$) Reaction at the B3LYP, QCISD and Single-Point CCSD(T)//B3LYP and CCSD(T)//QCISD Levels**

| species | B3LYP[a] | ZPVE/B3LYP[a] | CCSD(T)[b] //B3LYP[a] | total 1[c] | QCISD[a] | ZPVE/QCISD[a] | CCSD(T)[b] //QCISD[a] | total 2[d] | imag[e] |
|---|---|---|---|---|---|---|---|---|---|
| **R** ($NH_2^- + O_2$)[f] | 0.0 | 0.0 | 0.0 | 0.0 | 0.0 | 0.0 | 0.0 | 0.0 | |
| **P$_1$** ($O_2^- + NH_2$) | −36.3 | −0.4 | −23.1 | −23.5 | −28.6 | −0.3 | −22.6 | −22.9 | |
| **P$_2$** (HNO + $OH^-$) | −68.2 | 0.2 | −64.5 | −64.3 | −67.1 | 0.3 | −64.1 | −63.8 | |
| **P$_3$** ($NO_2^- + H_2$) | −21.4 | −3.7 | −13.8 | −17.5 | | | | | |
| **P$_4$** ($NO^- + H_2O$) | −67.3 | 1.5 | −71.5 | −70.0 | −67.7 | 1.8 | −71.1 | −69.4 | |
| **P$_5$** (c-$NO_2^- + H_2$) | 12.1 | −3.9 | 17.3 | 13.4 | | | | | |
| **P$_6$** ($ONO^- + H_2$) | −106.8 | −2.7 | −99.2 | −101.9 | | | | | |
| **1** | −63.8 | 5.1 | −56.1 | −51.0 | −55.6 | 5.5 | −55.6 | −50.1 | |
| **$^3$1** | −20.4 | 4.5 | −9.5 | −5.0 | | | | | |
| **2** | −78.8 | 2.1 | −67.8 | −65.7 | −66.5 | 2.5 | −67.3 | −64.8 | |
| **3** | −78.4 | 2.0 | −67.8 | −65.8 | | | | | |
| **4** | −18.4 | 4.0 | −11.5 | −7.5 | | | | | |
| **5** | −19.6 | 4.1 | −12.2 | −8.1 | | | | | |
| **6** | −18.4 | 4.0 | −11.5 | −7.5 | | | | | |
| **7** | 7.5 | −1.7 | 13.4 | 11.7 | | | | | |
| **8** | −95.4 | 3.3 | −85.3 | −82.0 | | | | | |
| **9** | −71.9 | 3.5 | −65.1 | −61.6 | | | | | |
| **10** | −100.4 | 1.6 | −93.6 | −92.0 | −95.4 | 1.7 | −93.8 | −92.1 | |
| **11** | −78.4 | 1.9 | −67.8 | −65.9 | | | | | |
| **12** | −100.5 | 1.3 | −94.9 | −93.6 | −96.0 | 1.5 | −94.4 | −92.9 | |
| **TS 1/2** | −41.5 | 1.5 | −36.1 | −34.6 | −32.0 | 1.7 | −35.5 | −33.8 | 1728.7i |
| **TS 1/4** | −10.7 | 1.3 | −3.5 | −2.2 | | | | | 1081.9i |
| **TS 1/6** | −10.7 | 1.3 | −3.5 | −2.2 | | | | | 1080.7i |
| **TS 1/7** | 23.8 | −1.6 | 31.0 | 29.4 | | | | | 617.8i |
| **TS1/P$_3$** | 0.3 | −1.5 | 11.9 | 10.4 | | | | | 655.6i |
| **TS 2/3** | −36.7 | 2.9 | −30.2 | −27.3 | | | | | 873.2i |
| **TS 2/10** | −78.3 | 1.8 | −69.4 | −67.6 | −74.7 | 0.3 | −70.4 | −70.1 | 200.4i |
| **TS 2/11** | −76.9 | 1.7 | −66.6 | −64.9 | | | | | 217.0i |
| **TS 4/5** | −8.7 | 3.2 | 1.3 | 4.5 | | | | | 751.0i |
| **TS 5/6** | −17.6 | 3.6 | −10.6 | −7.0 | | | | | 240.9i |
| **TS 6/3** | −15.6 | 3.2 | −12.0 | −8.8 | | | | | 657.0i |
| **TS 7/8** | 26.3 | −1.7 | 33.8 | 32.1 | | | | | 471.0i |
| **TS 8/9** | −47.4 | 1.2 | −41.6 | −40.4 | | | | | 1639.0i |
| **TS 9/10** | −47.1 | 2.0 | −38.0 | −36.0 | | | | | 507.3i |
| **TS 10/12** | −100.2 | 0.0 | −94.2 | −94.2 | −95.2 | 0.8 | −93.8 | −93.0 | 546.7i |
| **TS11/P$_3$** | −16.1 | −3.4 | −10.4 | −13.8 | | | | | 1151.7i |
| **TSP$_3$/P$_6$** | 11.5 | −4.4 | −4.2 | −8.6 | | | | | 926.7i |

[a] The basis set is 6-311++G(d, p) for B3LYP and QCISD, respectively. [b] The basis set is 6-311++G(3df, 2pd) for CCSD(T). [c] At the CCSD(T)/6-311++G(3df, 2pd)//B3LYP/6-311++G(d, p) + ZPVE level. [d] At the CCSD(T)/6-311++G(3df, 2pd)//QCISD/6-311++G(d, p) + ZPVE level. [e] At the B3LYP/6-311++G(d, p) level. [f] The total energy of reference reactants R at the B3LYP/6-311++G(d, p) level is −206.23435 au; at the CCSD(T)/6-311++G(3df, 2pd)//B3LYP/6-311++G(d, p) the level is −205.89603 au; at the QCISD/6-311++G(d, p) the level is −205.74368 au and at the CCSD(T)/6-311++G(3df, 2pd)//QCISD/6-311++G(d, p) the level is −205.89688 au, respectively; The ZPVE values at the B3LYP and QCISD levels are 0.02212 and 0.02222 au, respectively.

In addition, there are three other pathways to give **P$_2$** from complex **1**: first, **1** can cross a 1,2-H-shift barrier (48.8 kcal/mol) to form the intermediate **6** ($HNOHO^-$), then by the 2,3-H-shift and elongation of the O−O bond with a barrierless process to **3** before **P$_2$(4)**; second, **1** will cross a 1,2-H-shift barrier (48.8 kcal/mol) to form the intermediate **4** ($HNOHO^-$) which is a chiral isomer of **6**. After rotation of the N−H and O−H bonds, **4** can cross a barrier of 12.0 kcal/mol to form intermediate **5** ($HNOHO^-$). Followed by a torsion of N−H bond, **5** can pass a small barrier of 1.1 kcal/mol to form isomer **6** which will isomerize to **3** and then to **P$_2$** as listed in route **P$_2$(5)**; at last, **1** can take a concerted cleavage of N−H bond and cyclization of $NO_2^-$ with a barrier of 80.4 kcal/mol to gain the intermediate **7** (c-$O_2N\cdots H_2^-$). Then **7** can take concerted 1, 2-H-shift and O−O bond cleavage with a barrier of 20.4 kcal/mol to give weak-bound complex **8** ($ONH\cdots OH^-$) which could isomerize to **9** ($HONOH^-$) with a barrier of 41.6 kcal/mol corresponding to 1, 2-H-shift. Then **9** will experience a 1, 3-H-shift to form hydrogen-bond complex **10** with a barrier of 25.6 kcal/mol followed by **12** before **P$_2$** as listed in **P$_2$(6)**. It is clear that the rate-controlling step of the barrier (**1**→**2**, 16.4 kcal/mol) involved in pathway **P$_2$(1)** and **P$_2$(3)** is quite lower than the other four barriers of


dx.doi.org/10.1021/jp206518j |J. Phys. Chem. A 2011, 115, 13581–13588

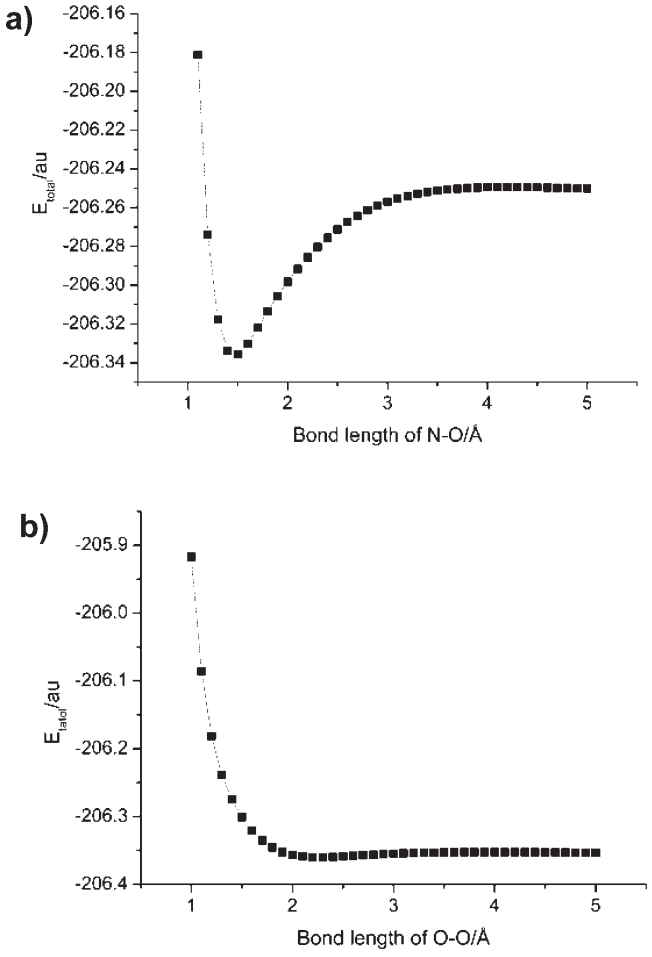


**Figure 4.** (a) Potential energy curve of reactants to intermediate **1** ($H_2NO_2^-$) at the B3LYP/6-311++G(d, p) level. The N−O bond of **1** ($H_2NO_2^-$) is elongated from 1.0 to 5.0 Å with stepsize of 0.1 Å, whereas the remaining geometrical parameters are fixed. (b) Potential energy curve of intermediate **2** ($HNO\cdots OH^-$) to $\mathbf{P_2}$ ($HNO + OH^-$) at the B3LYP/6-311++G(d, p) level. The O−O bond of **2** ($HNO\cdots OH^-$) is elongated from 1.0 to 5.0 Å with stepsize of 0.1 Å, whereas the remaining geometrical parameters are fixed.

38.4 (**2**→**3**) kcal/mol for $\mathbf{P_2(2)}$, 48.8 (**1**→**6**) kcal/mol for $\mathbf{P_2(4)}$, 48.8 (**1**→**4**) kcal/mol for $\mathbf{P_2(5)}$ and 80.4 (**1**→**7**) kcal/mol for $\mathbf{P_2(6)}$, respectively. In view of pathway of $\mathbf{P_2(1)}$ is quite simpler than $\mathbf{P_2(3)}$, it should be the most favorable pathway to $\mathbf{P_2}$.

$\mathbf{P_3}(NO_2^- + H_2)$

Starting from complex **1** ($H_2NO_2^-$), there are two pathways to generate $\mathbf{P_3}$ ($NO_2^- + H_2$) which can be described as follows:

$$\mathbf{P_3(1)} : \mathbf{R} \rightarrow \mathbf{1} \rightarrow \mathbf{P_3}$$

$$\mathbf{P_3(2)} : \mathbf{R} \rightarrow \mathbf{1} \rightarrow \mathbf{2} \rightarrow \mathbf{11} \rightarrow \mathbf{P_3}$$

At first, **1** ($H_2NO_2^-$) can take a $H_2$ elimination via a very high barrier of 61.4 kcal/mol leading to $\mathbf{P_3}$ ($NO_2^- + H_2$) directly as listed in path $\mathbf{P_3(1)}$. Alternatively, **1** can also convert to isomer **2**, subsequently via the rotation of O−O bond with a neglectable barrier of 0.8 kcal/mol to **11** ($HNO\cdots OH^-$), then take a concerted hydrogen-elimination from N−H and O−H bonds with a barrier of 52.1 kcal/mol to $\mathbf{P_3}$ ($NO_2^- + H_2$) as listed in path $\mathbf{P_3(2)}$. Note that in the path of $\mathbf{P_3(2)}$, there are three barriers to be surmounted, i.e., **TS1/2** (16.4 kcal/mol), **TS2/11** (0.8 kcal/mol), and $\mathbf{TS11/P_3}$ (52.1 kcal/mol), whereas the relative energy of 61.4 kcal/mol of $\mathbf{TS1/P_3}$ in the pathway $\mathbf{P_3(1)}$ is larger than any barrier in the path $\mathbf{P_3(2)}$. Therefore, the pathway of $\mathbf{P_3(2)}$ should be energetically more favorable than $\mathbf{P_3(1)}$.

$\mathbf{P_4}(NO^- + H_2O)$

Starting from the complex **1**($H_2NO_2^-$), there are two possible pathways to $\mathbf{P_4}$ ($NO^- + H_2O$), as listed below:

$$\mathbf{P_4(1)} : \mathbf{R} \rightarrow \mathbf{1} \rightarrow \mathbf{2} \rightarrow \mathbf{10} \rightarrow \mathbf{P_4}$$

$$\mathbf{P_4(2)} : \mathbf{R} \rightarrow \mathbf{1} \rightarrow \mathbf{7} \rightarrow \mathbf{8} \rightarrow \mathbf{9} \rightarrow \mathbf{10} \rightarrow \mathbf{P_4}$$

Once generation in the pathway of $\mathbf{P_2(3)}$ or $\mathbf{P_2(6)}$, **10** can take a N−H rupture easily leading to $\mathbf{P_4}$. The largest barriers involved in $\mathbf{P_4(1)}$ and $\mathbf{P_4(2)}$ are 16.4 and 80.4 kcal/mol, respectively. Therefore, $\mathbf{P_4(1)}$ is the favorable channel to $\mathbf{P_4}$.

$\mathbf{P_5}(c\text{-}NO_2^- + H_2)$

Note that both $\mathbf{P_5}$ ($c\text{-}NO_2^- + H_2$) and $\mathbf{P_3}$ ($NO_2^- + H_2$) include the dissociation product of $H_2$, and the difference just lies in that $NO_2^-$ of $\mathbf{P_5}$ ($c\text{-}NO_2^- + H_2$) is a three-membered ring structure while that of $\mathbf{P_3}$ ($NO_2^- + H_2$) is a bent form. Starting from **1** ($H_2NO_2^-$), only one pathway was found to $\mathbf{P_5}$ ($c\text{-}NO_2^- + H_2$), which is energetically very high-lying as 13.4 kcal/mol above reactants **R**:

$$\mathbf{P_5(1)} : \mathbf{R} \rightarrow \mathbf{1} \rightarrow \mathbf{7} \rightarrow \mathbf{P_5}$$

i.e., in the pathway $\mathbf{P_4(2)}$, **7** can alternatively take a concerted $H_2$-elimination and O−N−O cyclization to give $\mathbf{P_5}$ ($c\text{-}NO_2^- + H_2$) directly, which is an endothermic process.

$\mathbf{P_6}(ONO^- + H_2)$

It is clear that $\mathbf{P_6}$ ($ONO^- + H_2$) is the isomerization product of $\mathbf{P_3}$ ($NO_2^- + H_2$). The configuration of $ONO^-$ in $\mathbf{P_6}$ ($ONO^- + H_2$) is nitrite, which is different from cyclic $c\text{-}NO_2^-$ of $\mathbf{P_5}$ ($c\text{-}NO_2^- + H_2$) and bent $NO_2^-$ of $\mathbf{P_3}$. Actually, $\mathbf{P_6}$ ($ONO^- + H_2$) will be generated by the secondary reaction from $\mathbf{P_3}$ by undergoing an oxygen-shift transition state at 8.9 kcal/mol. Thus the reaction pathway of $\mathbf{P_6}$ ($ONO^- + H_2$) is just as follows:

$$\mathbf{P_6} : \mathbf{P_3} \rightarrow \mathbf{P_6}$$

## 4. REACTION MECHANISM

For the ion−molecule reaction of $NH_2^-$ with $O_2$ ($a^1\Delta_g$), totally six products from $\mathbf{P_1}$ to $\mathbf{P_6}$ on the singlet PES were predicted theoretically. From the analysis of the PES, the most feasible reaction pathways concerning every possible product are listed as follows:

$$\mathbf{P_1} : \mathbf{R} \rightarrow \mathbf{1} \rightarrow \mathbf{P_1}$$

$$\mathbf{P_2(1)} : \mathbf{R} \rightarrow \mathbf{1} \rightarrow \mathbf{2} \rightarrow \mathbf{P_2}$$

$$\mathbf{P_3(2)} : \mathbf{R} \rightarrow \mathbf{1} \rightarrow \mathbf{2} \rightarrow \mathbf{11} \rightarrow \mathbf{P_3}$$

$$\mathbf{P_4(1)} : \mathbf{R} \rightarrow \mathbf{1} \rightarrow \mathbf{2} \rightarrow \mathbf{10} \rightarrow \mathbf{P_4}$$

$$\mathbf{P_5} : \mathbf{R} \rightarrow \mathbf{1} \rightarrow \mathbf{7} \rightarrow \mathbf{P_5}$$

$$\mathbf{P_6} : \mathbf{P_3} \rightarrow \mathbf{P_6}$$

Note that the calculated the order of energy barriers of the rate-controlling step for above pathways increases as follows: $\mathbf{P_1}(0.0) < \mathbf{P_2(1)}(16.4) = \mathbf{P_4(1)}(16.4) < \mathbf{P_3(2)}(52.1) < \mathbf{P_5}(80.4)$. Hence, charge-transfer species $\mathbf{P_1}$ should be the most competitive product with the electron configurations of $O_2^-$ as $(1\sigma_g)^2(1\sigma_u)^2(2\sigma_g)^2(2\sigma_u)^2(3\sigma_g)^2(1\pi_u)^4(1\pi_g)^3$, and $NH_2$ as $(1a1)^2(2a1)^2(1b2)^2(3a1)^2(1b1)^1$. As shown in Figure 3, $\mathbf{P_2}$ lies 5.7(5.6) kcal/mol above $\mathbf{P_4}$, taking above kinetics into consideration, we believe that $\mathbf{P_4}$ should have a larger branching ratio than that of $\mathbf{P_2}$. So $\mathbf{P_4}$ should be the second feasible product followed by $\mathbf{P_2}$ as the third competitive product, and $\mathbf{P_3}$ may be the fourth feasible product with neglectable yield comparing with $\mathbf{P_1}$, $\mathbf{P_4}$, and $\mathbf{P_2}$ in view of its high barrier of rate-controlling step. Due to the fact that $\mathbf{P_5}$ (c-$NO_2^-$ + $H_2$) is the product of endothermic reaction, and $\mathbf{P_6}$ ($ONO^-$ + $H_2$) is just the secondary product of $\mathbf{P_3}$ ($NO_2^-$ + $H_2$), the observation of these two products experimentally is far more impossible. In order to check the reliability of B3LYP calculations, for the involved eleven species in the most favorable pathways $\mathbf{P_1}$, $\mathbf{P_2(1)}$ and $\mathbf{P_4(1)}$, the geometrical parameters and sing-point energies are refined at the QCISD/6-311++G(d, p) and CCSD(T)/6-311++G(3df, 2pd)//QCISD/6-311++G(d, p) levels, respectively. As shown in Table 1 as well as Figures 1, 2, and 3, the calculated geometrical parameters and single-point energies at the B3LYP and CCSD(T)//B3LYP levels are in great agreement with those of the QCISD and CCSD(T)//QCISD levels. Note that the largest relative energy difference between the CCSD(T)//B3LYP+ZPVE and CCSD(T)//QCISD+ZPVE levels is just 2.5 kcal/mol. So the present B3LYP and CCSD(T)//B3LYP calculations are reliable for the title reaction.

## 5. COMPARISON WITH EXPERIMENT

For $NH_2^-$ + $O_2$ ($a^1\Delta_g$) reaction, the only experimental study was carried out by Anthony Midey et al.[19] using selective ion flow tube (SIFT) technology in 2008. It is shown that the measured rate constant is very large as $9.0 \times 10^{-10}$ $cm^3s^{-1}$ at 300 K, which is consistent with our calculated low energy barriers to exothermic products $\mathbf{P_1}$, $\mathbf{P_2}$, and $\mathbf{P_4}$. Of course, for some competitive processes, it is desirable to perform kinetic calculations, while such studies are beyond the scope of the present paper. However, note that only two products, namely, $\mathbf{P_1}$ ($NH_2$ + $O_2^-$) and $\mathbf{P_2}$ (HNO + $OH^-$) were determined with the respective branching ratios at about 95% and 5% experimentally,[19] which is in contrast to our calculated results that $\mathbf{P_1}$ should be the primary product, while $\mathbf{P_4}$ ($NO^-$ + $H_2O$) and $\mathbf{P_2}$ (HNO + $OH^-$) may be the second and third favorable products with comparable yields. Therefore, further experimental investigation on the title reaction is very desirable.

## 6. CONCLUSIONS

The PES of ion−molecule reaction of $NH_2^-$ with $O_2$ ($a^1\Delta_g$) is theoretically studied for the first time at the B3LYP/6-311++G(d, p), QCISD/6-311++G(d, p) and sing-point CCSD(T)/6-311++G(3df, 2pd) levels of theory. On the singlet PES, it is shown that the barrierless association of $NH_2^-$ with $O_2$ ($a^1\Delta_g$) will generate a low-lying initial complexes, i.e., **1** ($H_2NO_2^-$), which will undergo a variety of isomerization and dissociation pathways to give six dissociation products, i.e., $\mathbf{P_1}$ ($NH_2$ + $O_2^-$), $\mathbf{P_2}$ (HNO + $OH^-$), $\mathbf{P_3}$ ($NO_2^-$ + $H_2$), $\mathbf{P_4}$ ($NO^-$ + $H_2O$), $\mathbf{P_5}$ (c-$NO_2^-$ + $H_2$), and $\mathbf{P_6}$ ($ONO^-$ + $H_2$). Among these products, the charge-transfer species $\mathbf{P_1}$ should be the primary product with predominant abundance followed by $\mathbf{P_4}$ and $\mathbf{P_2}$ as the second and third competitive products with few of $\mathbf{P_3}$; while $\mathbf{P_5}$ and $\mathbf{P_6}$ will not be produced due to either high isomerization barriers in pathway or being secondary products. It should be noted that only $\mathbf{P_1}$ ($NH_2$ + $O_2^-$) and $\mathbf{P_2}$ (HNO + $OH^-$) were detected in the experiment by Anthony Midey et al.[19] in 2008, whereas our theoretically predicted $\mathbf{P_4}$ ($NO^-$ + $H_2O$) was not found. So, the title reaction needs to be deeply explored by further experiments. We hope that the present theoretical study may be helpful for the understanding of the reaction mechanisms related to $NHX^-$, $NX_2^-$, $PHX^-$, and $PX_2^-$ (X = H, F, and Cl).

## AUTHOR INFORMATION

**Corresponding Author**
*E-mail: ghchen@stu.edu.cn.

## ACKNOWLEDGMENT

This work was supported by 211 project foundation of Guangdong Province. In addition, we owe a debt of gratitude to Miss Min-min Ma's help in polishing the English.

## REFERENCES

(1) Wayne, R. P. *Chemistry of Atmospheres*, 2nd ed.; Clarendon Press: Oxford, U. K., 1991.
(2) Bierbaum, V. M.; Schmitt, R. J.; DePuy, C. H. *Environ. Health Perspect.* **1980**, *36*, 119–134.
(3) McConnell, J. D. *J. Geophys. Res.* **1973**, *78*, 7812.
(4) Clarke, K.; Edge, R.; Johnson, V.; Land, E. J.; Navaratnam, S.; Truscott, T. G. *J. Phys. Chem. A.* **2008**, *112*, 1234–1237.
(5) Laszlo, B.; Alfassi, Z. B.; Neta, P.; Huie, R. E. *J. Phys. Chem. A.* **1998**, *102*, 8498–8504.
(6) Marcy, T. P.; Heard, D. E.; Leone, S. R. *J. Phys. Chem. A.* **2002**, *106*, 8249–8255.
(7) Wolf, M.; Yang, D. L.; Durant, J. L. *J. Phys. Chem. A.* **1997**, *101*, 6243–6251.
(8) Park, J.; Lin, M. C. *J. Phys. Chem. A.* **1997**, *101*, 2643–2647.
(9) Zhu, R. S.; Lin, M. C. *J. Phys. Chem. A.* **2007**, *111*, 3977–3983.
(10) Li, Q. S.; Lü, R. H. *J. Phys. Chem. A.* **2002**, *106*, 9446–9450.
(11) Inomata, S.; Washida, N. *J. Phys. Chem. A.* **1999**, *103*, 5023–5031.
(12) Adamson, J. D.; Farhat, S. K.; Morter, C. L.; Glass, G. P.; Curl, R. F.; Phillips, L. F. *J. Phys. Chem.* **1994**, *98*, 5665–5669.
(13) Miller, J. A.; Klippenstein, S. J. *J. Phys. Chem. A.* **2000**, *104*, 2061–2069.
(14) Okada, S.; Abe, Y.; Yamabe, S. *J. Phys. Chem.* **1995**, *99*, 16877–16882.
(15) Peräkylä, M. *J. Phys. Chem.* **1996**, *100*, 3441–3447.
(16) Eyet, N.; Midey, A.; Bierbaum, V. M.; Viggiano, A. A. *J. Phys. Chem. A.* **2010**, *114*, 1270–1276.
(17) Upschulte, B. L.; Marinelli, W. J.; Green, B. D. *J. Phys. Chem.* **1994**, *98*, 837.
(18) Evans, W. F. J.; Hunten, D. M.; Llewellyn, E. J.; Jones, A. V. *J. Geophys. Res.* **1968**, *73*, 2885.
(19) Midey, A.; Dotan, I.; Seeley, J. V.; Viggiano, A. A. *Int. J. Mass Spectrom.* **2009**, *280*, 6–11.
(20) Frisch, M. J.; Trucks, G. W.; Schlegel, H. B.; Scuseria, G. E.; Robb, M. A.; Cheeseman, J. R.; Zakrzewski, V. G.; Montgomery, J. A. Jr.; Stratmann, R. E.; Burant, J. C.; Dapprich, S.; Millam, J. M.; Daniels, A. D.; Kudin, K. N.; Strain, M. C.; Farkas, O.; Tomasi, J.; Barone, V.; Cossi, M.; Cammi, R.; Mennucci, B.; Pomelli, C.; Adamo, C.; Clifford, S.; Ochterski, J.; Petersson, G. A.; Ayala, P. Y.; Cui, Q.; Morokuma, K.; Malick, D. K.; Rabuck, A. D.; Raghavachari, K.; Foresman, J. B.; Cioslowski, J.; Ortiz, J. V.; Stefanov, B. B.; Liu, G.; Liashenko, A.; Piskorz, P.; Komaromi, I.; Gomperts, R.; Martin, R. L.; Fox, D. J.; Keith, T.; Al-Laham, M. A.; Peng, C. Y.; Nanayakkara, A.; Gonzalez, C.;

Challacombe, M.; Gill, P. M. W.; Johnson, B. G.; Chen, W.; Wong, M. W.; Andres, J. L.; Head-Gordon, M.; Replogle, E. S.; Pople, J. A. *Gaussian03*, revision C.02; Gaussian, Inc.: Pittsburgh, PA, 2003.
(21) Becke, A. D. *J. Chem. Phys.* **1993**, *98*, 5648.
(22) Lee, C.; Yang, W.; Parr, R. G. *Phys. Rev. B.* **1988**, *37*, 785.
(23) Hehre, W. J.; Ditchfield, R.; Pople, J. A. *J. Chem. Phys.* **1972**, *56*, 2257.
(24) Krishnan, R.; Binkley, J. S.; Seeger, R.; Pople, J. A. *J. Chem. Phys.* **1980**, *72*, 650.
(25) Li, Y.; Liu, H. L.; Sun, Y. B.; Li, Z.; Huang, X. R.; Sun, C. C. *J. Phys. Chem. A.* **2010**, *114*, 2874–2884.
(26) Fukui, K. *Acc. Chem. Res.* **1981**, *14*, 363.
(27) Raghavachari, K.; Trucks, G. W.; Pople, J. A.; Head-Gordon, M. *Chem. Phys. Lett.* **1989**, *157*, 479.
(28) Scuseria, G. E.; Schaefer, H. F., III *J. Chem. Phys.* **1989**, *90*, 3700.
(29) Li, Y.; Liu, H. L.; Huang, X. R.; Wang, D. Q.; Sun, C. C.; Tang, A. C. *J. Phys. Chem. A.* **2008**, *112*, 12252–12262.
(30) Pople, J. A.; Head-Gordon, M.; Raghavachari, K. *J. Chem. Phys.* **1987**, *87*, 5968.
(31) Curtiss, L. A.; Raghavachari, K.; Redfern, P. C.; Rassolov, V.; Pople, J. A. *J. Chem. Phys.* **1998**, *109*, 7764.